Numerical considerations of fluid effects on wave propagation: Influence of the tortuosity

E. H. Saenger, O. S. Krüger, and S. A. Shapiro

email: *saenger@geophysik.fu-berlin.de*

keywords: *Gassmann equation, Biot's velocity relations, dry and fluid-saturated rocks, rotated staggered grid, finite differences, numerical rock physics*

ABSTRACT

The focus of this paper is on effective elastic properties (i.e. velocities) in three different kinds of dry and fluid-saturated porous media. The synthetic results are compared with the predictions of the Gassmann equation and the tortuosity-dependent high-frequency limit of the Biot velocity relations. Using a dynamic FD approach we observe for Fontainebleau sandstone the same effective elastic properties as with a static finite-element approach. We show that so-called open-cell Gaussian random field models are similar in mechanical properties to Fontainebleau sandstone. For all synthetic models considered in this study the high-frequency limit of the Biot velocity relations is very close to the predictions of the Gassmann equation. However, using synthetic rock-models saturated with an imaginary fluid of high density we can approximately estimate the corresponding tortuosity parameter.

INTRODUCTION

The problem of effective elastic properties of dry and fluid-saturated porous solids is of considerable interest for geophysics, material science, and solid mechanics. Strong scattering caused by complex rock structures can be treated only by numerical techniques since an analytical solution of the wave equation is not available. In this paper we consider the problem of a porous medium in three dimensions. Alternative numerical studies of elastic moduli of porous media of Arns et al. (2002) and Roberts and Garboczi (2002) employ a (static) finite-element method (FEM). This FEM uses a variational formulation of the linear elastic equations and finds the solution by minimizing the elastic energy using a fast conjugate-gradient model. Dynamic effects (e.g. velocity dispersion) can not be described with this method. Finite difference (FD) methods discretize the wave equation on a grid. They replace spatial derivatives by FD operators using neighboring points. This discretization can cause instability problems on a staggered grid when the medium contains high contrast discontinuities (e.g. pores or fractures). These difficulties can be avoided by using the rotated staggered grid (RSG) technique (Saenger and Bohlen (2004) and references therein). Since the FD approach is based on the wave equation without physical approximations, the method accounts not only for direct waves, primary and multiply reflected waves, but also for surface waves, head waves, converted reflected waves, and diffracted waves. The main objective of this paper is a numerical study of effective elastic properties of porous 3D-media with connected dry and fluid-filled pores. The synthetics are compared with the high and low frequency limit of the Biot's theory in dependence of the tortuosity α (Biot, 1956).

THE SYNTHETIC MODELS OF POROUS ROCKS

In order to consider fluid effects on wave propagation we design a number of synthetic rock-models (size: 400^3 gridpoints) with a known number of pores or porosity ϕ. We consider three different types (i.e.

	MEDIUM:	GRF 1	GRF 2	GRF 3	GRF 4	GRF 5
	Porosity ϕ:	3.42%	8.77%	13.2%	8.02%	21.6%
Gaus. A	corrl. len. $[0.0002m]$	25	25	25	13	25
	cut min.	0.4	0.4	0.4	0.4	0.38
	cut max.	0.6	0.6	0.6	0.6	0.62
Gaus. B	corrl. len. $[0.0002m]$	30	30	30	15	14
	cut min.	0.485	0.48	0.4575	0.4904	0.46
	cut max.	0.515	0.52	0.5415	0.5296	0.54

Table 1: Details of the open-cell GRF models. Every single model (GRF1-5) is build up of the intersection of two two-level cutted Gaussian random fields (Gaussian A and B).

geometries):

- Type 1: A homogeneous region is filled at random with randomly oriented non-intersecting thin penny-shaped pores. The effective elastic properties of those materials are intensively investigated in Saenger et al. (2004). However, we include some results of this numerical study in the present paper to give a relation to other pore geometries.

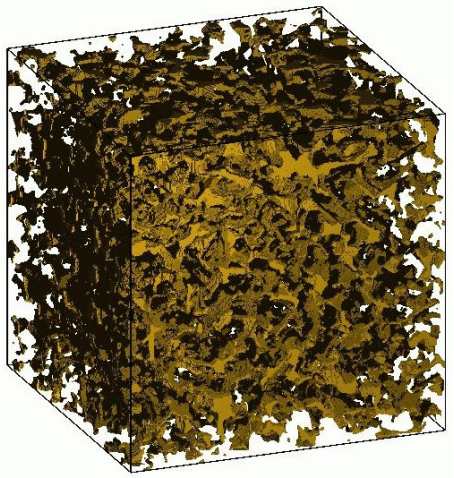

Figure 1: X-ray microtomographic image of Fontainebleau sandstone (used by Arns et al. (2002), originally from Spanne et al. (1994); porosity $\phi = 8.4\%$). The structure shown is the porespace, the transparent part is the grain material.

- Type 2: The second type of model is a microtomographic image of Fontainebleau sandstone shown in Figure 1. We use a 400^3 gridpoint cubic data set of the model fb7.5 of Arns et al. (2002). Therefore, the numerical estimates of effective elastic properties derived with the RSG-based dynamic FD approach can be compared with the results of the static approach of Arns et al. (2002).

- Type 3: To generate realistic synthetic microstructures we use the approach described in Roberts and Garboczi (2002), the so-called open-cell Gaussian random field (GRF) scheme. The porespace is defined by the intersection of two two-cutted Gaussian random fields (i.e. Gaussian A and Gaussian B; see Table 1 for details). To ensure a complete connectivity of the pores we eliminate isolated pores. This connectivity is a basic assumption of the Gassmann equation (see e.g. Wang (2000)). Figure 2 shows one typical realization.

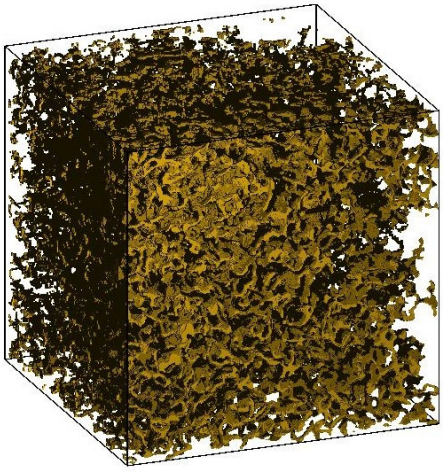

Figure 2: An open-cell Gaussian random field (GRF 4) with a porosity $\phi = 8\%$. The similarity between this model and the Fontainebleau sandstone (Figure 1) is evident. The similarity can also be observed for the effective elastic properties (see Figures 3 and 4).

MODELING PROCEDURE

We apply the RSG-technique to model wave propagation in porous media. The synthetic rock-models (type 1,2 and 3) are embedded in a homogeneous region. The full models are made up of 804x400x400 grid points with an interval of 0.0002m. In the homogeneous region and for the grain material we set a P-wave velocity of v_p=5100m/s, a S-wave velocity of v_s=2944m/s and a density of ρ_{grain}=2540kg/m^3. For the dry pores we set v_p=0m/s, v_s=0m/s and ρ_v=0.0001kg/m^3 which approximates vacuum. For the fluid-filled pores we set v_p=1500m/s, v_s=0m/s and ρ_{fl}=1000kg/m^3 which approximates water. We perform our modeling experiments with periodic boundary conditions in the two horizontal directions. To obtain effective velocities in different models we apply a body force plane source at the top of the model. The plane P- or S-wave generated in this way propagates through the porous medium. With two horizontal planes of receivers at the top and at the bottom, it is possible to measure the time-delay of the mean peak amplitude of the plane wave caused by the inhomogeneous region. With the time-delay one can estimate the effective velocity and therefore also the corresponding elastic moduli. The source wavelet in our experiments is always the first derivative of a Gaussian with a dominant frequency of $8 * 10^4 Hz$ and with a time increment of $\Delta t = 2.1 * 10^{-9} s$. All computations are performed with second order spatial FD operators and with a second order time update. A similar numerical setup with a detailed error analysis is discussed in Saenger et al. (2004).

NUMERICAL RESULTS

Our numerical setup enables us to compare effective elastic properties of dry and fluid filled 3D porous media (i.e. the dry rock skeleton is exactly the same in both cases). Therefore we can test the applicability of the Gassmann-equation and the Biot velocity relations (Gassmann, 1951; Biot, 1956) for our 3D porous materials without any additional effective medium theory. For all synthetic models we fulfill the following assumptions of the Gassmann equation: isotropy, frictionless fluid, undrained system, and no chemical interactions (discussed e.g. by Wang (2000)). However, from a theoretical point of view we consider here the high frequency range of the Biot velocity relations because we saturate our rock-models with a non-viscous fluid (: viscosity $\eta = 0$; hence, the reference frequency f_{biot} can be determined for our rock-models with a non-zero permeability κ using $f_{biot} = \phi\eta/(2\pi\rho_{fl}\kappa)$ as zero; see e.g. Mavko et al. (1998)). Note, there is one geometrical parameter in the Biot velocity relations, namely the tortuosity parameter α, which is not easy to determine analytically. The difference between the high frequency limit and the low frequency limit (i.e. Gassmann equation) of the Biot velocity relations for the fast P- and the S-wave is maximal for α=1 and is zero for $\alpha \rightarrow \infty$. This can be easily evaluated for S-waves by analyzing the

corresponding prediction of the Biot approach (e.g. Mavko et al. (1998)):

$$V_{S\infty} = \left(\frac{\mu_{dry}}{\rho - \phi \rho_{fl} \alpha^{-1}} \right)^{\frac{1}{2}}, \tag{1}$$

where $V_{S\infty}$ is the high frequency limiting velocity, μ_{dry} is the effective shear modulus of the dry rock skeleton, ρ_{fl} is the fluid density, and ρ is the density of the whole porous material $[\rho = (1-\phi)\rho_{grain} + \phi\rho_{fl}]$. The much more complicated formula for the velocity of the fast P-wave with the tortuosity-behavior described above can also be found in Mavko et al. (1998). Another important solid-fluid interaction is the Squirt mechanism (Mavko et al. (1998) and references therein). The reference frequency for this fluid-flow is given by $f_{squirt} = K_{grain} a^3/\eta$ where K_{grain} is the bulk modulus of the grain material and a is the pore aspect ratio. The use of a non-viscous fluid ($\eta = 0$) in this work means that our modeling takes place in the zero freqency limit in respect to the Squirt theory. Thus, from three distinct solid-fluid interactions (viscous Biot-coupling, Squirt flow and inertial coupling) we work with the inertial coupling only. However, our numerical results provide asymptotic values for all three coupling mechanism.

Penny-shaped cracks

The calculated effective moduli for fluid-filled and for empty non-intersecting cracks (model Type 1) are shown for two different realizations in Figure 3 and 4. Detailed results for these kind of media and other structures with thin cracks can be found in Saenger et al. (2004) and Orlowsky et al. (2003). The main point here is the relation to the pore structures discussed below.

Fontainebleau Sandstone

The calculated normalized effective shear moduli $< \mu > /\mu_{grain}$ for the dry and fluid-saturated Fontainebleau sandstone (model Type 2) are 0.766 and 0.770, respectively (see Figure 3). In spite of the high-frequency limit of Biot theory, where our numerical results apply, the prediction of the Gassmann equation ($\mu_{dry} = \mu_{sat}$) is for this model very accurate. This is a first indication that the tortuosity α must be relatively high. Only in this case the numerical considered high frequency limit of the Biot approach is close to Gassmann. Moreover, our dynamic approach gives approximately the same result as the static approach of Arns et al. (2002) [$< \mu > /\mu_{grain} \approx 0.765$, for the dry and fluid-saturated case from Fig. 5b of Arns et al. (2002)]. One more remarkable aspect of these considerations for Fontainebleau sandstone is that the connectivity of the pores is not complete (but rather 95%) which is in principle inconsistent with one of assumptions of the Gassmann equation.

Open-cell Gaussian random fields (GRF)

The calculated effective moduli for the open-cell Gaussian random field models are shown in Figure 3 and 4. With an increase of the porosity (GRF 1, 4, 2, 3 and 5) we observe an increasing mismatch between the predictions of the Gassmann equation ($\alpha \to \infty$) and the numerical results. Again, we expect this behavior because we consider here numerically the tortuosity-dependent high frequency limit of the Biot approach. In particular for the effective elastic shear moduli of the fluid-saturated models GRF 2,3 and 5 (see Figure 3) one can pre-estimate a tortuosity α relatively close to 1. However, for the model GRF 4 (porosity $\phi = 8\%$) we obtain very similar effective elastic properties as for Fontainebleau sandstone (porosity $\phi = 8.4\%$).

Tortuosity determination using an imaginary fluid of high density for saturation

For all examples discussed above the difference between the high and the low frequency limit of the Biot velocity relations is relatively low. To distinguish numerically non-ambiguously between both limits we saturate the synthetic rock models with an imaginary fluid of high density [$v_p = 1500m/s$, $v_s = 0m/s$ and $\rho_{fl} = 15000kg/m^3$ (!)]. For such models the difference between both limits increases significantly (Figure 5 and 6). Moreover, we can fit the high frequency limit of the Biot velocity relations to numerical results by varying the tortuosity parameter α. The best fit for the tortuosity from the numerically estimated

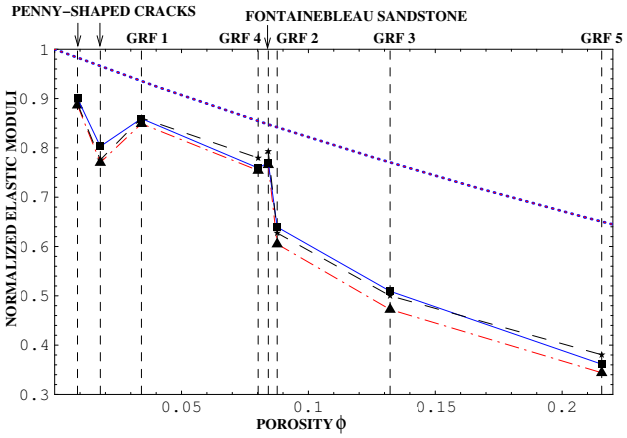

Figure 3: Normalized effective shear moduli ($< \mu > / \mu_{grain}$; with μ_{grain} as shear modulus of the grain material) versus porosity for eight different synthetic rock-models. $< \mu >_{dry}$ [triangles joined with a dashed-dotted line] and $< \mu >_{sat}$ [boxes joined with a solid line] are estimated from numerical velocity measurements for the dry and water-saturated case, respectively. The high-frequency limit of the Biot velocity relations [tortuosity α=1; stars joined with a black dashed line] is calculated using $< \mu >_{dry}$. The blue dotted line displays the upper Hashin-Shtrikman bound (Hashin and Shtrikman, 1963).

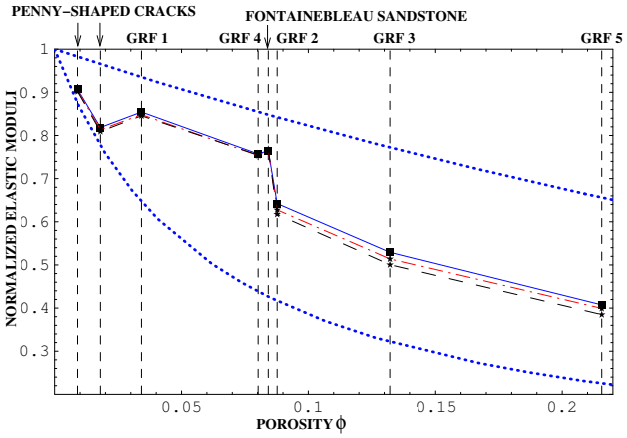

Figure 4: Normalized effective bulk moduli ($< K > / K_{grain}$; with K_{grain} as bulk modulus of the grain material) versus porosity for eight different synthetic rock- models. $< K >_{sat}$ [boxes joined with a solid line] is estimated from numerical velocity measurements for the water-saturated case. $K_{Gassmann}$ [stars joined with a dashed-dotted line] is calculated using the Gassmann-equation with $< \mu >_{dry}$ and $< K >_{dry}$. The high-frequency limit of the Biot velocity relations [tortuosity α=1; stars joined with a dashed line] is also calculated using $< \mu >_{dry}$ and $< K >_{dry}$. The dotted lines display the Hashin-Shtrikman bounds for the water-saturated case.

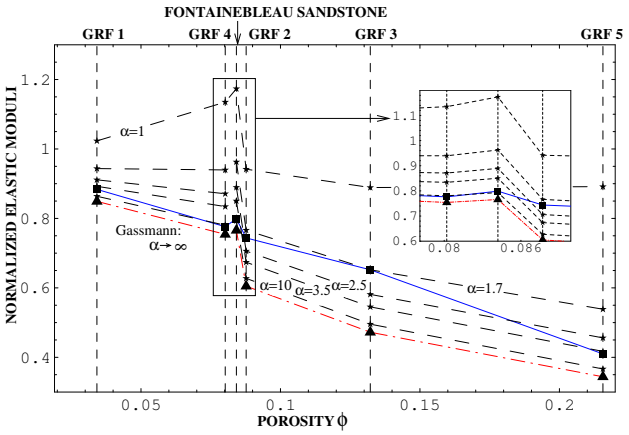

Figure 5: The normalized effective shear moduli ($< \mu > /\mu_{grain}$) versus porosity for six different models saturated with an imaginary fluid of high density ($\rho_{fl} = 15000 kg/m^3$) are shown (boxes joined with a solid line). The dashed lines display the high frequency limit of the Biot approach using different values for the tortuosity α.

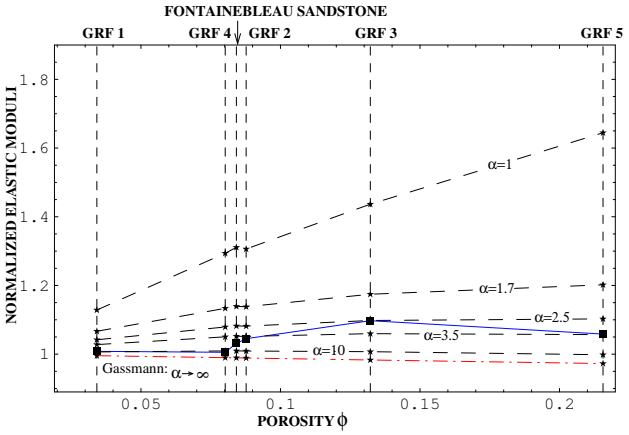

Figure 6: The normalized effective bulk moduli ($< K > /K_{grain}$) versus porosity for six different models saturated with an imaginary fluid of high density are shown (boxes joined with a solid line). The dashed lines display the high frequency limit of the Biot approach using different values for the tortuosity α.

values of $< \mu >$ and $< K >$ are listed in Table 2. They are in a qualitative agreement with the theoretical prediction of Berryman (1981). For spherical inclusions he suggests the relation α=0.5(1+1/ϕ). It is obvious that there is not a better agreement because the geometry used in the models is more complex than spherical inclusions. However, from our point of view it is important to show that values of the tortuosity α over 6 are reasonably for the low-porosity models used here. Another confirmation of our Biot-based tortuosity determination of the Fontainebleau sandstone sample can be found in Arns et al. (2001). They determine numerically for exact the same Fontainebleau sandstone speciment a reciprocal formation factor of $F^{-1} \approx (2.6 \pm 2.6) * 10^{-3}$ (see Fig. 2 of Arns et al. (2001)). Using the fact that the formation factor F is related to the tortuosity α via $F = \alpha/\phi$ (Walsh and Brace, 1984) one can calculate a tortuosity of $\alpha \approx 32$. Note, the accuracy of tortuosity determination for relatively high values (α above 6) is limited. Therefore, our results ($\alpha \approx 7.5$; see Table 2) are in a qualitative agreement with Arns et al. (2001).

CONCLUSIONS

We use the rotated staggered finite-difference grid technique to calculate elastic wave propagation in 3D porous media. Our numerical modeling of elastic properties of isotropic dry and fluid-saturated rock skeletons can be considered as an efficient and well controlled computer experiment. Using this approach it is

	α from $<\mu>$	α from $<K>$	$\overline{\alpha}$	α_{th}
GRF 1	5	10	7.5	15
GRF 4	10	10	10	6.7
Font. Sandst.	10	5	7.5	6.4
GRF 2	2	2.8	2.4	6.2
GRF 3	1.7	2.5	2.1	4.3
GRF 5	3.5	3.5	3.5	2.8

Table 2: Numerical estimates of the tortuosity parameter α from Figure 5 and 6. $\overline{\alpha}$ is the arithmetic average. For comparison, we also give an theoretical porosity-dependent estimate of the tortuosity α_{th} by Berryman (1981).

possible to predict precisely effective elastic moduli of various pore geometries in the relatively wide range between the upper and lower Hashin-Shtrikman bound. We have tested the applicability of the Gassmann equation and the tortuosity-dependent Biot velocity relations to three different types of porous media. For the Fontainebleau sandstone model we confirm the estimates of elastic properties obtained in Arns et al. (2002). For this model the Gassmann equation can be verified because of the relatively high tortuosity. Additionally, we show that so-called open-cell Gaussian random field models are realistic synthetic rock-models useful for studying fluid effects on wave propagation in porous media. The theoretically predicted high-frequency limit of the Biot approach can clearly be observed. With rock-models saturated with an imaginary fluid of high density we can roughly estimate the tortuosity parameter α of those materials.

ACKNOWLEDGEMENTS

This work was kindly supported by the sponsors of the *Wave Inversion Technology (WIT) Consortium*, Berlin, Germany.

REFERENCES

Arns, C. H., Knackstedt, M. A., and Pinczewski, W. V. (2001). Accurate estimation of transport properties from microtomographic images. *Geophys. Res. Lett.*, 28:3361–3364.

Arns, C. H., Knackstedt, M. A., Pinczewski, W. V., and Garboczi, E. J. (2002). Computation of linear elastic properties from microtomographic images: Methodology and agreement between theory and experiment. *Geophysics*, 67:1396–1405.

Berryman, J. G. (1981). Elastic wave propagation in fluid-saturated porous media. *J. Acoust. Soc. Amer.*, 69:416–424.

Biot, M. A. (1956). Theory of propagation of elastic waves in a fluid-saturated porous solid. I. Low frequency range and II. Higher-frequency range. *J. Acoust. Soc. Amer.*, 28:168–191.

Gassmann, F. (1951). Über die Elastizität poröser Medien. *Vier. der Natur Gesellschaft*, 96:1–23.

Hashin, Z. and Shtrikman, S. (1963). A variational approach to the elastic behavior of multiphase materials. *J. Mech. Phys. Solids*, 11:127–140.

Mavko, G., Mukerji, T., and Dvorkin, J. (1998). *The Rock Physics Handbook*. Cambridge University Press, Cambridge.

Orlowsky, B., Saenger, E. H., Guéguen, Y., and Shapiro, S. A. (2003). Effects of parallel crack distributions on effective elastic properties - a numerical study. *International Journal of Fractures*, 124(3-4):L171–L178.

Roberts, A. P. and Garboczi, E. J. (2002). Computation of the linear elastic properties of random porous materials with a wide variety of microstructure. *Proc. R. Soc. Lond. A*, 458:1033–1054.

Saenger, E. H. and Bohlen, T. (2004). Anisotropic and viscoelastic finite-difference modeling using the rotated staggered grid. *Geophysics*, 69(2):583–591.

Saenger, E. H., Krüger, O. S., and Shapiro, S. A. (2004). Effective elastic properties of randomly fractured soils: 3D numerical experiments. *Geophys. Prosp.*, 52(3):183–195.

Spanne, P., Thovert, J., Jacquin, J., Lindquist, W. B., Jones, K., and Coker, D. (1994). Synchotron computed microtomography of porous media. *Phys. Rev. Lett.*, 73:2001–2004.

Walsh, J. B. and Brace, W. F. (1984). The effect of pressure on porosity and the transport properties of rock. *J. Geophys. Res.*, 89:9425–9431.

Wang, Z. (2000). *The Gassmann Equation Revisited: Comparing Laboratory Data with Gassmann's Predictions*, pages 8–23. Society of Exploration Geophysics.